ELSEVIER

Journal of Molecular Catalysis A: Chemical 168 (2001) 193–207

JOURNAL OF MOLECULAR CATALYSIS A: CHEMICAL

www.elsevier.com/locate/molcata

Cobalt–aluminum co-precipitated catalysts and their performance in the Fischer–Tropsch synthesis

Alexander A. Khassin*, Tamara M. Yurieva, Galina N. Kustova, Izabella Sh. Itenberg, Margarita P. Demeshkina, Tamara A. Krieger, Lyudmila M. Plyasova, Galina K. Chermashentseva, Valentin N. Parmon

Boreskov Institute of Catalysis, 5, Pr. Lavrentieva, Novosibirsk 630090, Russia

Received 21 June 2000; accepted 6 November 2000

Abstract

Cobalt–aluminum catalysts were prepared using either Co^{2+} precipitation onto freshly prepared Mg–Al or Zn–Al hydrotalcite (promoted samples) or co-precipitation of Co^{2+} and Al^{3+} (non-promoted samples). The evolution of initial hydrotalcite structure was monitored during its calcination and reductive treatment. It has been shown that, at moderate temperatures, hydrotalcites results decomposition yields a Co oxide phase supported by a highly defective inverted spinel-like structure. Cations Co^{2+} enter the support structure, and occupy both tetrahedral and octahedral positions. Octahedron coordinated Co species are reduced at 580–620°C. After the reduction at 470–480°C catalyst phase composition shows Co^0 supported on inverted spinel-like structure, which contains Co^{2+} in the octahedral coordination. Further reduction at 600°C transforms the support to 'ideal' spinel, which contains no octahedron coordinated Co^{2+}. Chemical properties of the Co–Al catalysts, including their performance in the Fischer–Tropsch synthesis (FTS), were found to depend on the catalyst reduction temperature, and thus on the support structure. Metal-support interaction is supposed to explain the observed properties of metallic cobalt.

Keywords: Cobalt; Spinels; Alumina; Fischer–Tropsch; Metal-support interaction

1. Introduction

Cobalt–alumina catalysts are well known to be active in hydrogenation reactions, CO hydrogenation to hydrocarbons (the Fischer–Tropsch synthesis, FTS) in particular. There are many papers reporting on the properties of these catalysts in the FTS [1–6]. Some of them discuss catalyst deactivation under reaction conditions (see for example [4]). Deactivation of Co–Al catalysts is attributed to the oxidation of Co^0 species by water molecules, which are the primary FTS product. It may be assumed that Co^0 is oxidized to Co^{2+} cations, which are located in the surface octahedrons of alumina support. Other studies report on the effect of catalyst preparation conditions on the extent of Co species reduction in Co–Al catalysts [5–8]. However, further investigations are necessary to clarify the nature of interaction between the Co^{2+} cations and the support.

Here we report on the model cobalt–aluminum catalysts, prepared by either precipitaion of Co^{2+} onto freshly prepared Mg–Al or Zn–Al hydrotalcite (promoted samples) or co-precipitation of Co^{2+} and Al^{3+} (unpromoted samples). Investigation focuses on the

* Corresponding author. Tel.: +7-383-2-344109; fax: +7-383-2-343056.
E-mail address: yurieva@catalysis.nsk.su (A.A. Khassin).

1381-1169/01/$ – see front matter
PII: S1381-1169(00)00529-X

Table 1
The composition and the way of preparation of the catalyst samples under the study

Sample	Composition	Way of preparation	Conditions
ZA	Zn:Al = 1:2	Coprecipitation of Me^{2+} and Al^{3+} from 10 wt.% aqueous solution of the corresponding nitrates	pH 6.6; 70°C; NH_4HCO_3
MA	Mg:Al = 1:2		pH 10; 65°C; NaOH and Na_2CO_3 (1:5) mixture
CA	Co:Al = 1:2		pH 7.5; 60°C; Na_2CO_3
CA-I	Co:Al = 1:1, 3		
CA-II	Co:Al = 1:1		
N/CA	Co:Al = 1:1	Incipient wetness impregnation of dried CA sample by the aqueous solution of Co nitrate	
P/MA	Co:Mg:Al = 1:1:2	The same as for the MA (ZA) sample, but followed by precipitation of Co^{2+} from a nitrate aqueous solution	pH 7.5; 60°C; Na_2CO_3
P/ZA	Co:Zn:Al = 1:1:2		pH 7.5; 60°C; Na_2CO_3

nature of the interaction between Co^{2+} species and hydroxycompounds of Al and promoting metal, on the effect of support composition and its structure on the reducibility of Co species, as well as on the catalytic properties of Co–Al catalysts. Below are investigation results related to the structural evolution of Co–Al precipitated catalysts during their activation, and to their catalytic performance in FTS.

2. Experimental section

2.1. Preparation of the catalysts

Eight samples were prepared. Table 1 presents their composition and their preparation procedure. Precipitation was performed from a stoichiometric 10 wt.% aqueous solution of corresponding nitrates ('pure for chemical analysis' grade, Uralian plant of chemicals, Russia) at 60–70°C. A mixture of 7.5 wt.% water solutions of NaOH and Na_2CO_3 or 7.5 wt.% water solution of NH_4HCO_3 were used as precipitants. Precipitated catalysts were washed thoroughly by distilled water, and dried overnight under an IR lamp in air. Catalyst N/CA, prepared by an incipient wetness impregnation, was dried overnight under the IR lamp in air.

2.2. Characterization techniques

In situ thermal gravimetry (STA) data were obtained by means of a Netzsch STA 409 thermal balance. The sensitivity of weight determining was about 0.1 mg (approximately 0.1% of the sample weight). Heating rate was $10\,K\,min^{-1}$ at measurements in argon flow and in air, and it was $5\,K\,min^{-1}$ at measurements in hydrogen flow. Parameters for the STA TPR studies were optimized in order to minimize criterion P defined in [9,10]: $P = \beta S_0/FC_0$, where β is the heating rate ($K\,min^{-1}$); F the flow rate ($ml\,min^{-1}$); C_0 the initial H_2 concentration ($mol\,ml^{-1}$); S_0 the amount of reducible species in the sample (mol). The value of P should be at least lower than 20 K. In our studies $P \approx 5^*(5 \times 10^{-4})/150/(4.5 \times 10^{-5}) \approx 1.7$ K.

The accuracy of determining Co reduction degree by means of temperature programmed reduction and temperature programmed oxidation STA measurements may be estimated as ca. 10%.

X-ray diffraction (XRD) studies were done with Siemens D-500 diffractometer using the Cu Kα radiation. Ex situ XRD measurements of calcined and reduced samples were done in air soon after samples exposure to air. In situ measurements were held in a homemade chamber described elsewhere [11].

Infrared transmission spectra (IRS) were recorded in a range of 300–4000 cm^{-1} by FTIR spectrometer Bomem MB-102. Powdered catalyst samples were diluted with CsI (or KBr), or the catalyst powder emulsions were prepared using a fluorinated oil.

For calcination and reduction, we used 99.99% purity Ar and 99.9% purity H_2, which were additionally purified from O_2 traces to 0.1 ppm over a Ni–Cr catalyst, and also from water by silica gel.

2.3. Catalytic tests

Catalytic tests were held in a slurry reactor under atmospheric pressure ($P = 1.2$–1.3 atm), and H_2:CO ratio at reactor inlet was 2. *N*-tetradecane, *n*-$C_{14}H_{30}$, was used as a filling. Slurry temperature was varied from 463 to 503 K with an accuracy of ±1 K. Inlet gas also contained 10% of N_2 used as internal standard.

Slurry volume was 20 ccm, and catalyst sample weight varied from 1 to 2 g. Catalyst powder with particles less than 0.18 mm was used for the purpose. Inlet gas velocity was varied from 0.3 to 1.2 l h^{-1}, which seemed to have no influence on the catalyst activity or selectivity. Gas feed was organized under a single bubble regime, average bubble diameter being ca. 0.2 mm, and residence time being ca. 3 s. The mass transfer coefficients of reactants in the slurry could be estimated by the Mu–Yang model [12] as 0.03–0.04 cm s^{-1}, so the value of ($k_L a$) was 50 times higher than the observed rates of CO conversion. This fact evidences that reactant diffusion is not the rate limiting stage (here *a* is the area of gas bubbles, which are resident in the slurry at a given moment).

Product was analyzed regarding gaseous products (C_1–C_8), condensate (C_8–C_{15}) and hydrocarbon fraction C_{11+} dissolved in the slurry. These products were analyzed with TSVET-530 (USSR) chromatograph equipped by a column packed with γ-Al_2O_3 (fraction C_1–C_8) and with TSVET-560 (USSR) chromatograph equipped by a glass capillary with phase SE-30 (for the C_{8+} fractions). As proved by special tests, the values of the Anderson–Schultz–Flory (ASF) parameter α, calculated from the C_2–C_8 fraction and from the C_{15+} fraction (dissolved in the slurry), differed by less than 0.02, which is close to the measurements accuracy. So, α-value was usually calculated solely from the data on fraction C_2–C_8.

The relative accuracy of methane formation rate in a single measurement was ±18%. With five measurements it was possible to achieve an accuracy of ±11%. The relative accuracy of CO conversion rate determining was rather poor and equaled ±25%. This accuracy could be improved to ±20% by making several measurements. When determining the ASF parameter α, accuracy was much better, since not the absolute values, but only the ratio of C_{n+1} and C_n formation rates was important. Thus, the accuracy of α-value determining was ±0.015.

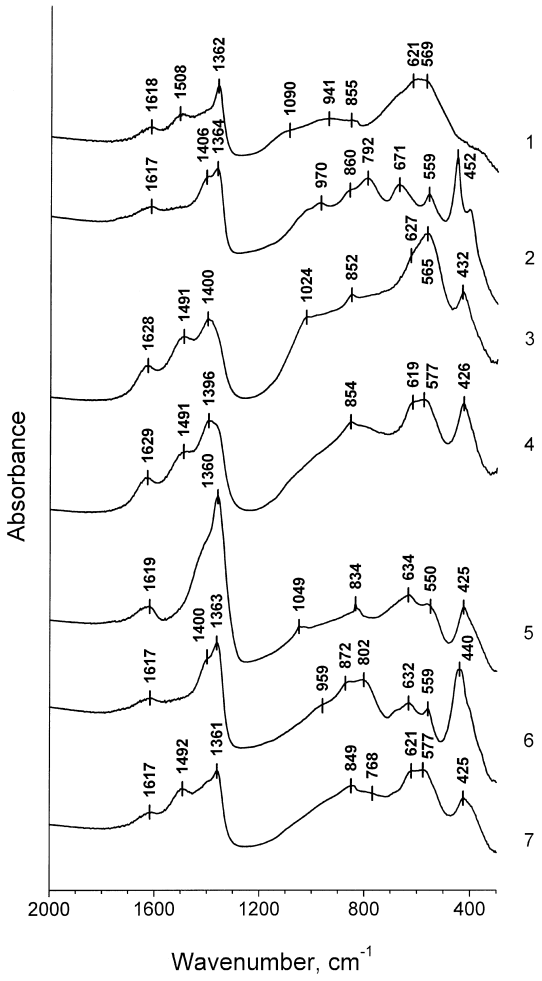

Fig. 1. IR spectra of the uncalcined samples under study: 1, ZA; 2, MA; 3, CA; 4, CA-II; 5, N/CA; 6, P/MA; 7, P/ZA.

3. Results and discussion

3.1. Characterization of catalysts

3.1.1. Uncalcined catalysts

The IR spectra of uncalcined samples were registered to determine their phase composition (see Fig. 1). According to [13–15] these spectra evidence, that all dry samples seem to contain the phase of a hydrotalcite-type structure. Absorption bands at 350–600 cm^{-1} are attributed to the lattice vibrations of cations, those at ca. 620–635 cm^{-1} to Me^{2+}–Al–OH bend vibrations, at ca. 660–680 cm^{-1}

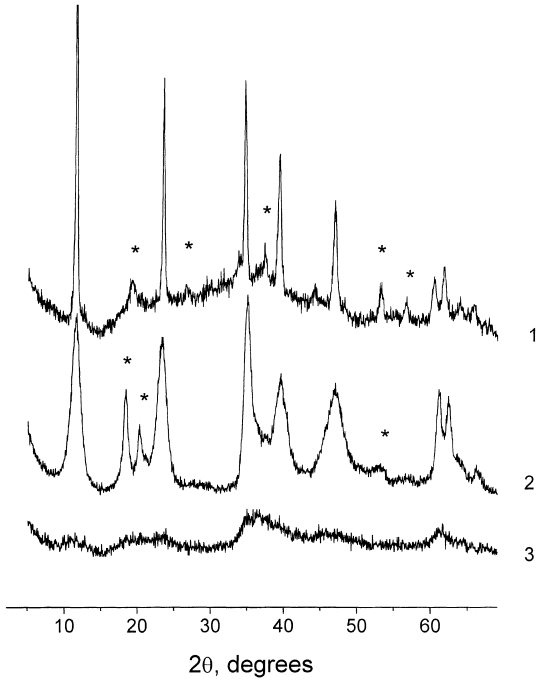

Fig. 2. The XRD patterns of the uncalcined samples: 1, ZA; 2, MA; 3, CA. Asterisks show the peaks which are not attributed to the hydrotalcite-type phase.

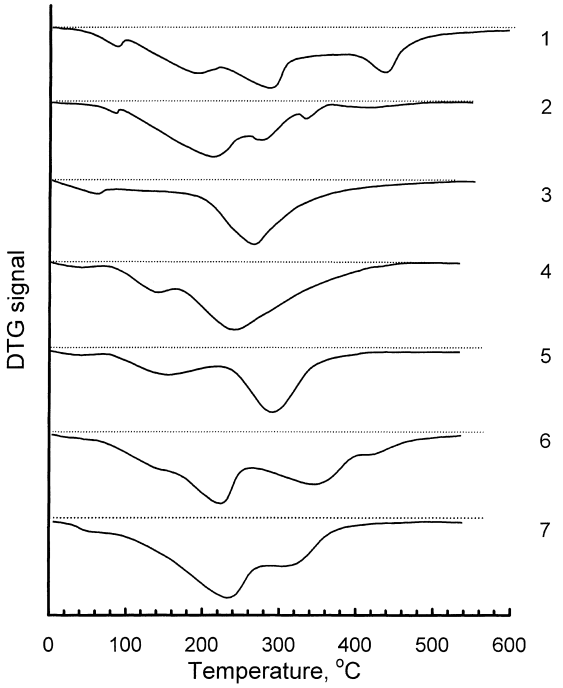

Fig. 3. STA data (DTG, solid line; DTA, dashed line) on the calcination of the samples: 1, MA; 2, ZA; 3, CA; 4, CA-II; 5, N/CA; 6, P/MA; 7, P/ZA.

to Me^{2+}–Al–OH stretch vibrations. Vibrations of hydrotalcite lattice CO_3^{2-} groups are registered at 620–635 (ν_4), 835–875 (ν_2), 1020–1100 (ν_1) and 1350–1420 cm^{-1} (ν_3). Indistinct bands at 900–1050 cm^{-1} are attributed to δ Al–OH vibrations. Bands at ca. 1617 or 1629 apparently belong to δ vibrations of H_2O molecules. Carbonate groups, adsorbed on the sample surface, are characterized by the distinct band at 1490–1520 cm^{-1} (ν_3 CO_3^{2-}).

Conclusion about hydrotalcite-like structure generation agrees with the XRD data (see Fig. 2). An important difference of the observed IRS spectra from those, reported in [13,14] for hydrotalcites with stoichiometry Me:Al = 6:2, is a much higher intensity of Al–OH absorption bands with respect to Me^{2+}–OH absorption bands. One may explain this difference by a small content of divalent cations in the samples under the study.

According the XRD data, $Zn(OH)_2$ or $Al(OH)_3$ are also present in the samples ZA or MA, correspondingly. For sample N/CA, vibrations of NO_3^- group in $Co(NO_3)_2{\cdot}6H_2O$ are present at the IR spectrum (see a higher intensity of absorption band 1360 cm^{-1}). Normally, anion NO_3^- is characterized by absorption at ca. 1358 cm^{-1} [16].

3.1.2. Calcination of the catalysts in the inert gas flow

Catalysts calcination in the inert gas flow causes decomposition of precursor compounds. Experimental STA profiles are given in Fig. 3. They are similar to those reported earlier for hydrotalcites of Mg and Co with stoichiometry Me:Al = 6:2 [13]. However, weight loss effects (curves in Fig. 3) are shifted to higher temperatures, and are not well resolved, since temperature increment rate is relatively high. According to [13], hydrotalcite-type structure decomposition proceeds in two steps: CO_3^{2-} groups removal (decarbonylation) and OH^- groups removal (dehydroxylation). The STA profiles of the MA and ZA sample show an apparent non-homogeneity of these samples, since three or even four weight loss effects may be seen in these profiles, while only two can be expected for the hydrotalcite-type structure decomposition.

Actually, phase ZnO [17] (or MgO [18], or CoO [19]) is detected by the XRD of sample MA (or ZA or CA) after its calcination at 250°C in air for 4 h. Dehydroxylation of hydrotalcites should not proceed at such a low temperature. This indicates that corresponding phase $Me(OH)_x(CO_3)_y$ is obviously present in the uncalcined samples.

CO_3^{2-} removal from the hydrotalcite structure leads to its transformation to cubic structure (NaCl-type), keeping layered structure, however (see the study of Cu–Zn–Al hydrotalcites in [20]). Two peaks at 2θ ca. 13 and 19° stay in the patterns of samples ZA and MA. Two halos at 2θ ca. 35 and 65° are present in the pattern of MA, indicating the cubic NaCl-type structure. Most likely samples ZA and CA already have 'spinel-like' cubic structure (or a 'protospinel' structure, see [21]), since a partial dehydroxylation of the MA sample occurs at 250°C already.

The XRD patterns of samples after calcination at 500°C show no peaks, assigned to the hydrotalcite-type structure. For all samples, XRD reveals a poorly-crystallized spinel phase (see Fig. 4, curves 2–7). The spinel-like phase lattice parameter could be adequately determined only for samples ZA (a = 8.079 Å), MA (a = 8.007 Å), and CA (a = 8.081 Å). These phases cannot be identified without the IRS data, and will be discussed later.

In sample N/CA well-crystallized Co_3O_4 spinel phase (a = 8.080 Å) co-exists with amorphous spinel. In samples ZA, MA, CA-*, P/ZA and M/ZA phase $Me^{2+}O$ is present. The quantity of this divalent metal oxide is different, particularly, there is a lot of ZnO and MgO in samples ZA and MA, but only traces of CoO are found in sample CA. The lattice parameter of MeO phase in sample P/MA is equal to that reported in [18] for pure MgO (a = 4.214 Å). Taking into account that the lattice parameter of mixed Co–Mg oxide depends almost linearly on the Co^{2+} content [22,34] and reaches 4.26 Å for pure CoO [19], one may conclude that there is no significant introduction of Co^{2+} into the Mg oxide. The analysis of the XRD pattern of sample P/MA cannot exclude a presence of an amorphous (or dispersed) CoO phase. For samples CA-* lattice parameter of phase MeO, a = 4.25 Å indicates that this phase is a solution of some Mg^{2+} cations in the CoO oxide structure.

The IRS data on the calcined samples are present in Figs. 5 and 6 and in Table 2. Fig. 5 shows the IRS data

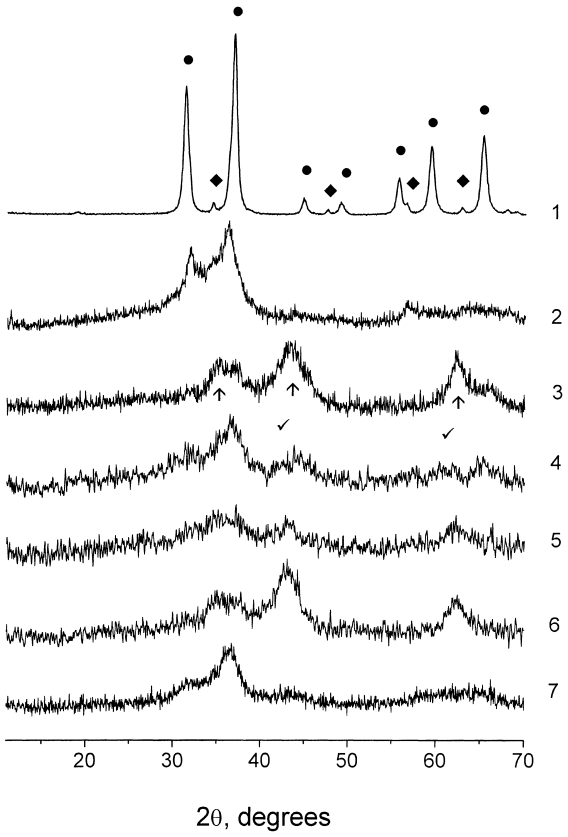

Fig. 4. The XRD pattern of the calcined Al-containing samples: 1, ZA calcined at 800°C; 2, ZA calcined at 500°C; 3, MA calcined at 800°C; 4, CA calcined at 500°C; 5, CA-II calcined at 500°C; 6, P/MA calcined at 500°C; 7, P/ZA calcined at 500°C; (●), spinel phase; (◆), ZnO; (↑), MgO; (✓), CoO.

evolution for samples MA and CA during their calcination. IRS data evolution for sample ZA is similar to that of sample CA. Fig. 6 shows the most important IRS spectra of other calcined samples under the study. The IR spectrum of MA and ZA samples calcined at 250°C differs from that of corresponding hydrotalcites (see Fig. 5, curves 1 and 2). The intensity of absorption bands at ca. 1500, 1400, 1020, 870, 670 and 560 cm^{-1} diminished strongly, thus, indicating the removal of a significant amount of groups CO_3^{2-} and OH^-. Bands at ca. 790 and 630 cm^{-1} are shifted to higher frequencies. Spectrum transformation continues at sample calcination at 500°C (CA sample, Fig. 5, curve 5) or at 800°C (MA sample, Fig. 5, curve 3). These spectra show three wide bands within 400–900 cm^{-1}.

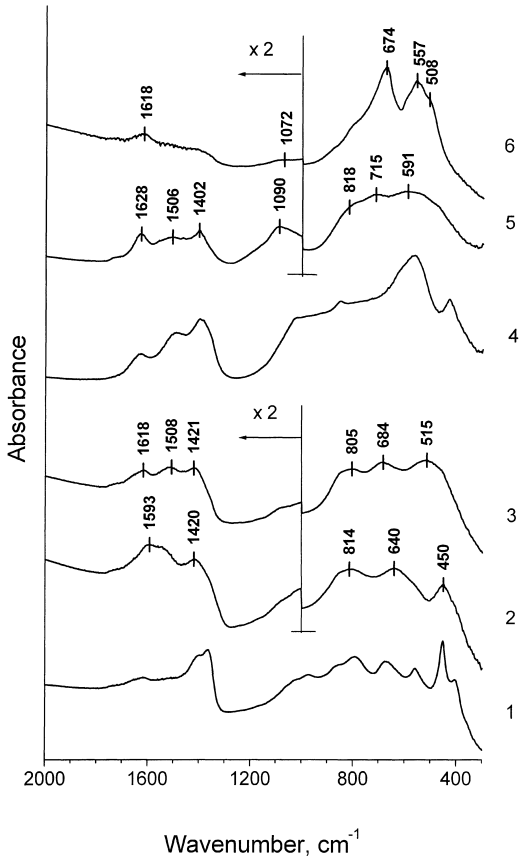

Fig. 5. The evolution of the IR spectra of the samples MA and CA during the calcination in the Ar flow. Sample MA: 1, uncalcined; 2, calcined at 250°C; 3, calcined at 800°C. Sample CA: 4, uncalcined; 5, calcined at 500°C; 6, calcined at 800°C.

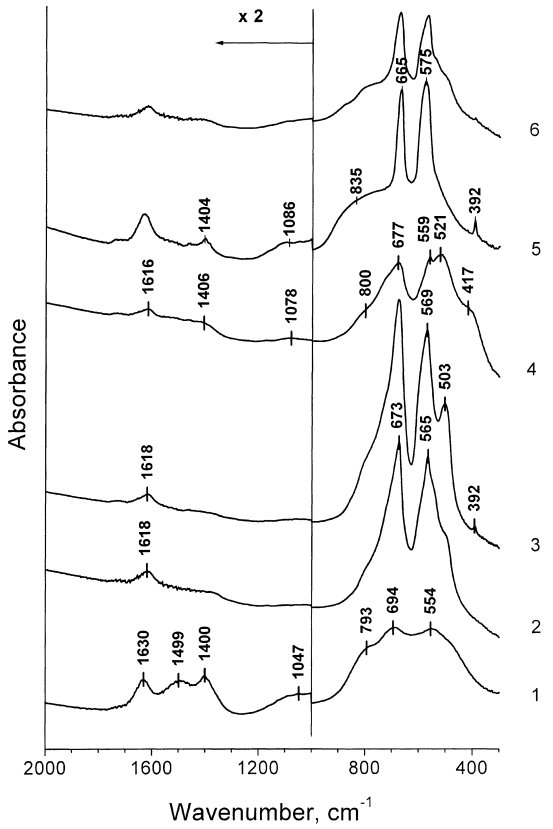

Fig. 6. The IRS data on the calcined samples: 1, P/ZA calcined at 500°C; 2, P/ZA calcined at 800°C; 3, P/ZA calcined at 500°C, then reduced at 650°C and oxidized at 700°C; 4, P/MA calcined at 1000°C; 5, N/CA calcined at 500°C; 6, N/CA calcined at 800°C.

Absorption maxima positions are far from those typical for corresponding aluminates, as reported in (see Table 2). Bands at ca. 1070, 1420 and 1520 cm^{-1} undoubtedly show OH^- and CO_3^{2-} groups to be still present in the 'spinel-like' phase.

It has been shown in [24] that bands at 550–600, 650–720 and 780–820 cm^{-1} may be attributed to inverted spinel structure, where some Al^{3+} cations occupy tetrahedral positions. Our IR data on samples MA calcined at 800°C, as well as on ZA, CA and CA-II calcined at 500°C are similar to those reported in [24] for the Me^{2+}–Al^{3+} oxides with inverted cationic distribution, in particular, for a $(Mg_{1/2}Al_{1/2})Al_{1.83}\square_{0.17}O_4$ ($\square$ is a cationic vacancy) non-stoichiometric spinel. In our case, spinel phase inversion cannot be attributed to the non-stoichiometric composition of samples: the IR spectra change dramatically after samples calcination at high temperatures (see below). In addition, for sample CA-II, ratio Co^{2+}:Al^{3+} is above the stoichiometry. Thus, we ascribe the Me–Al spinel inversion to the presence of anionic admixtures, which distort the spinel structure, and make tetrahedral positions more favorable for cations Al^{3+} than oxygen coordinated tetrahedrons in the ideal (high-temperature) spinel.

On further calcination of samples CA and ZA intensity of above mentioned absorption bands, related to the OH^- and CO_3^{2-} groups, decreases. The position of bands for sample ZA calcined at 800°C shows that, it consists of 'ideal' $ZnAl_2O_4$ phase. Sample CA after the calcination at 800°C seems to be $CoAl_2O_4$, however its distortion is significant (see Fig. 5, curve

Table 2
Experimental data on the position of the IR absorption band maxima (cm^{-1}) of the samples under the study

Sample	Temperature of calcination (°C)	Absorption band positions (cm^{-1})					
$MgAl_2O_4$	[23]	309	522	580	688	–	
	250	–	450	–	640	814	1019
MA	800	–	515	–	684	805	1073
$ZnAl_2O_4$	[23]	227	518	575	690	–	
	250	–	–	551	669	818	1035
ZA	500	–	–	590	679	783	1090
	800	226	504	560	680	–	1125
$CoAl_2O_4$	[23]	237	523	563	684	–	
	500	–	–	591	715	818	1090
CA	800	225	508	557	674	–	1072
CA-II	500	–	513	619	–	801	

6). In addition, traces of above described 'spinel-like' phase are still present in the sample, indicating that spinel phase inversion has not yet disappeared totally. Sample MA contains no 'ideal' $MgAl_2O_4$ phase even after its calcination at 800°C (see Fig. 5, curve 3).

Thus, according to the IRS data, hydrotalcite-type structure transformation into Me^{2+} aluminate proceeds gradually via a 'spinel-like' phase. The IR spectra of 'spinel-like' phase show band at ca. 800 cm^{-1}, which should be attributed to the removal of the degeneracy of the Al–O vibration bands, and is related to a partial inversion of spinel structure (see Figs. 5 and 6). In addition, a significant amount of the OH^- and CO_3^{2-} groups is present in the structure of 'spinel-like' phase, as it can be seen from IR spectra within 1000–1600 cm^{-1}. Concerning the XRD data described above, one may note that there are two effects, which influence the lattice parameter of 'spinel-like' phase. They are: (i) a deficit of Me^{2+} to form stoichiometric aluminate, which diminishes the lattice parameter; (ii) anionic admixtures like the OH^- and CO_3^{2-} groups, which increase the lattice parameter value. Thus, 'spinel-like' phase lattice parameter values may vary in a wide range (see for example [25–27]), making no contradiction with the XRD data.

The structure of phase under discussion was earlier attributed (e.g. for the Mg-containing sample) to $MgAl_2O_4$ [13] and $(Mg_{1/2}Al_{1/2})Al_{1.83}\square_{0.17}O_4$ [24]. According to the present data, we ascribe it to the inverted spinel structure with a composition of $(Me^{2+}{}_{1-x}Al^{3+}{}_x)(Me^{2+}{}_xAl^{3+}{}_{2-x})O_{4-y-z}(OH^-)_{2y}(CO_3^{2-})_z$. Note that, for the normal oxygen coordination, the octahedron site preference energy of the Al^{3+} cation is ca. 54 kJ mol^{-1} relatively to the Co^{2+} cation (see [8,28]). Thus, a significant inversion of 'ideal' spinel phase structure is not thermodynamically favorable. However, spinel phase inversion may be caused by anionic admixtures present in its structure, as it was reported earlier for Cu-containing spinels in [25,27].

According to IRS, samples CA and ZA transform to the corresponding aluminates during their calcination at 800°C. The evolution of aluminum-containing phase structure in samples P/MA, P/ZA and N/CA seems to be similar to that described above.

3.1.3. Reduction of cobalt containing catalysts calcined at 500°C

Experimental STA TPR profiles of samples calcined at 450–500°C are shown in Fig. 7. Two main regions of samples weight loss are obviously distinguished: in a range of 200–500°C, as well as in a range of 500–700°C.

Earlier, the TPR profiles of Co/Al_2O_3 catalysts were studied in details by Arnoldy and Moulijn in [8] for sample 9.1% Co/Al_2O_3 prepared via impregnation with Co^{2+} nitrate. Four ranges of Co reduction were observed. Region I (250–370°C) was attributed to reduction of Co_3O_4 and CoO, and is very similar to the STA effects in Fig. 7. Region II (ca. 470°C) was attributed to reduction of Co^{3+} from a Co_2Al-oxide phase; no reduction in this range was observed in the present study. Region III (ca. 600°C) was assigned to reduction of Co^{2+} in surface positions of the support.

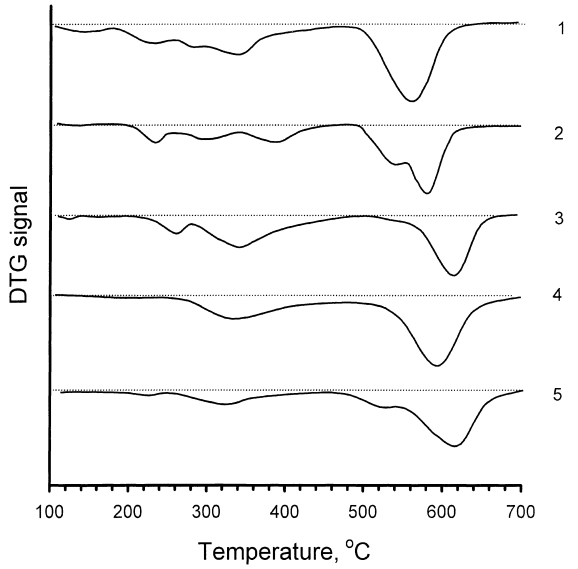

Fig. 7. STA data on the reduction in the hydrogen flow of the samples precalcined in the flowing inert gas: 1, CA; 2, CA-II; 3, N/CA; 4, P/MA; 5, P/ZA.

A similar attribution of Co/Al_2O_3 catalyst reduction at 600°C was reported in [4]. However, it is evident that this attribution cannot be regarded as consistent with our data. Weight loss effect is too large to be ascribed to the surface transformations. According to the data of [8] $CoAl_2O_4$ reduction occurs at 850–950°C (region IV).

In [7], the amount of Co^{2+} species reduced at 500–600°C in Co/Al_2O_3 was shown to increase after impregnated sample treatment with mixture $H_2 + H_2O$ at 350°C. In [1], reduction of impregnated catalyst Co/Al_2O_3 at 560°C was attributed to that of Co^{3+} in the octahedral positions of $CoAl_2O_4$.

Further, we shall use the data of [8] regarding hydrogen consumption during reduction at 600°C, which was measured to be $1H_2$ molecule per 1Co atom reduced, indicating that Co^{2+} species are indeed reduce in this region.

Normally, the Co_3O_4 spinel phase reduces either at ca. 280°C in a single step yielding Co^0 or in two steps at 250°C and at 350°C yielding CoO and Co^0, correspondingly (note that despite several explanations given for experimental data contradictions, its nature is still unclear). Apparently, weight loss by samples N/CA and P/ZA within 200–500°C should be attributed to reduction of Co_3O_4 (or $Zn_xCo_{3-x}O_4$) to CoO (or $Co_{1-x}Zn_xO$) and, then, to metallic Co^0. We also intend to attribute at least a part of low-temperature weight loss of samples CA and CA-II to reduction of Co_3O_4. As for sample P/MA, its weight loss at ca. 350–400°C should be attributed to reduction of $Co_{1-x}Mg_xO$.

We attribute weight loss at ca. 600°C to reduction of Co^{2+} in the octahedral positions of inversed 'spinel-like' phase accompanied by a simultaneous removal of the OH^- and CO_3^{2-} groups.

The XRD patterns of samples reduced at 470–480°C (as well as of those reduced at 600°C) show the peaks from β-Co^0 phase. The IRS data show a small amount of Co_3O_4 phase in the samples, first reduced at 470–480°C and then exposed to air for several hours.

Table 3
The estimated extent of the Co reduction according to the TPR STA measurements[a]

Sample	Co loading[b] (wt.%)	The extent of Co reduction below 500°C (%)	The extent of Co reduction at 500–700°C (%)
CA	37	32[c]	163[e]
CA-I	46	25[c]	84[e]
CA-II	54	35[c]	84[e]
N/CA	54	68[c]	109[e]
P/MA	29	74[d]	237[e]
Z/MA	24	68[c]	195[e]

[a] The values are given with respect to the total Co loading.

[b] The calculated loading of Co in the 'totally' reduced sample, which consists of Co^0, Al^{3+}, Mg^{2+}, Zn^{2+} and O^{2-} species and is free of the OH^- and CO_3^{2-} groups.

[c] Calculated in the supposition that Co_3O_4 transforms into Co^0 during the reduction and O^{2-} transforms into H_2O.

[d] Calculated in the supposition that CoO transforms into Co^0 during the reduction and O^{2-} transforms into H_2O.

[e] Calculated in the supposition that Co^{2+} transforms into Co^0 and O^{2-} transforms into H_2O.

We believe Co_3O_4 oxide to form via the oxidation of dispersed Co^0 by atmospheric oxygen.

TPR STA profiles allow us to estimate the amount of reduced Co during the low-temperature reduction of samples (see Table 3). We estimate assuming that weight loss results from Me_xO_y reduction to Me^0 producing H_2O. However, according to Table 3, this hypothesis is not consistent with experiment, at least for the high temperature reduction. It is evident that OH^- and CO_3^{2-} removal is expected to occur at 500–700°C. Actually, the latter assumption agrees with the IRS data on reduced samples: reduction at temperatures above 600°C causes the decrease of absorption bands intensity within 1000–1600 cm^{-1} (despite the fact that they do not vanish completely).

Temperature-programmed oxidation of reduced samples by static air was used in order to correct the estimation of reduction degree and to study the accessibility of Co^0 surface to molecules from the gas phase.

3.1.4. Reoxidation of the catalysts

The STA profiles of reduced samples reoxidaiton are shown in Fig. 8. Reoxidation was performed in the static air. The profiles of reoxidation of samples, prereduced at temperatures above 600°C show three distinct effects. Two low-temperature effects of weight gain in a range of 100–250°C are caused by the Co_3O_4 formation from the Co^0 particles, which are easily accessible to gaseous molecules. Weight gain at 500–600°C and higher temperatures we attribute to the oxidation of encapsulated cobalt particles. Necessity for O_2 molecules to penetrate through the $(Me_x)AlO_y$ phase barrier significantly decreases the rate of Co^0 oxidation at low and moderate temperatures.

The amount of Co^0 in reduced samples may be estimated from the total weight gain during the temperature programmed oxidation treatment. The estimated values are given in Table 4. It is assumed that Co^0 transforms to Co_3O_4 during the oxidation. It is quite natural to suppose that 'encapsulated' Co^0 particles, which may be oxidized at 500–600°C, will not be active in the FTS. Experimental data on the amount of 'accessible' Co^0 are also presented in the Table 4.

Reoxidation profiles of samples, reduced at 470–480°C, differ from the above discussed profiles by a significant shift of positions of maxima from the weight gain effects to higher temperatures.

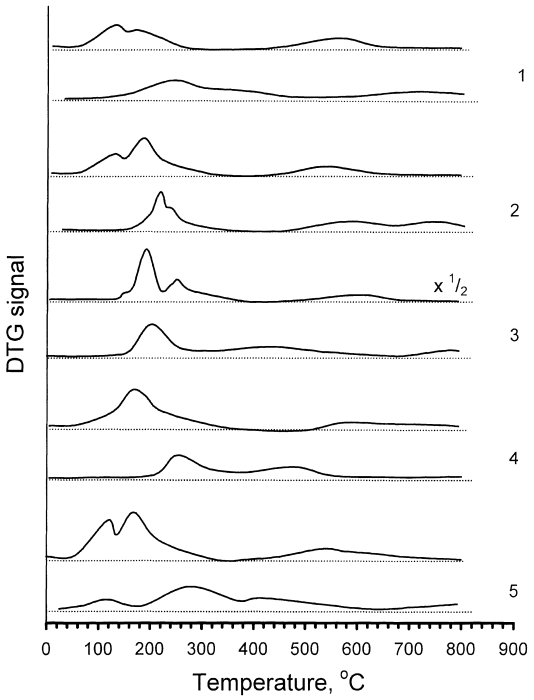

Fig. 8. STA data on the reoxidation of the samples prereduced at 600–650°C (the upper curve) and at 470–480°C (the lower curve): 1, CA; 2, CA-II; 3, N/CA; 4, P/MA; 5, P/ZA.

Co^0 phase dispersion can hardly cause the observed shift of reoxidation temperature. Since Co^0 may be expected to be better dispersed in the samples reduced at lower temperatures, oxidation temperature is expected to shift to lower temperatures, i.e. contradicting experimental fact. It is quite natural to relate the observed difference in the oxidation maxima positions to some changes in the structure of catalyst supports. We have mentioned above that OH^- and CO_3^{2-} groups removal occurs at 600°C in hydrogen medium. If this is the case, the shifted positions of oxidation maxima are the important indication to the 'metal-support' interaction for the $Co/\{(Me^{2+}_{1-x}Al^{3+}_x)(Me^{2+}Al^{3+}_{2-x})O_{4-y-z}(OH)_{2y}(CO_3^{2-})_z\}$ catalysts, which should be taken into consideration during catalyst performance analysis. Please note that reoxidation profiles of impregnated sample N/CA are the same for samples reduced at 480 and 600°C.

Reduction extent of unpromoted (CA) samples is far below 100%. Only ca. 70% of Co loading can be

Table 4
The estimated amount of oxidized Co according to the STA measurements[a]

Sample	Temperature of reduction	Amount of Co^0, Co loading (%)	Amount of 'accessible' Co^0, Co loading (%)
CA	470	11	6
	600	35	15
CA-II	480	34	19
	600	63	51
N/CA	480	58	51
	600	84	68
P/MA	480	56	35
	600	115	78
Z/MA	470	76	61
	600	108	65

[a] The values are given with respect to the total Co loading.

reduced in samples P/MA and P/ZA at 470–480°C. However, the reduction extent of P/MA and P/ZA after the reduction at 600°C is obviously close to 100% (estimation gives values above 100%). Thus, one may conclude that:

- cations Co^{2+} are incorporated in $(Me^{2+}{}_{1-x}Al^{3+}{}_{x})(Me^{2+}Al^{3+}{}_{2-x})O_{4-y-z}(OH)_{2y}(CO_3{}^{2-})_z$ support of calcined catalysts P/MA and P/ZA, and occupy octahedral positions;
- Mg^{2+} and Zn^{2+} present in the support structure help a total reduction of Co^{2+} in support $(Me^{2+}{}_{1-x}Al^{3+}{}_{x})(Me^{2+}Al^{3+}{}_{2-x})O_{4-y-z}(OH)_{2y}(CO_3{}^{2-})_z$, i.e. all cations Co^{2+} are located in the octahedral positions, and no cations Co^{2+} are located in the tetrahedral positions.

3.2. Catalytic tests

3.2.1. Catalytic tests of the catalysts reduced at 580–630°C

The results of the catalytic tests of catalysts reduced at 580–630°C in pure hydrogen flow are present in Table 5. Note the following peculiarities of catalysts performance. All catalysts exhibit a high selectivity to heavy hydrocarbons. Experimental values of α agree with the earlier hypothesis on the effect of Co^0 particles size on Co^0 selectivity in FTS [30,31]. The highest selectivity was achieved with CA, CA-I and CA-II (unpromoted) catalysts, possessing smaller Co^0 particles in reduced state.

On the other hand, non-promoted catalysts are not very active. This may be caused by a low degree of cobalt reduction in these samples, and by a low amount of 'accessible' cobalt. Cobalt reducibility increases with increasing Co loading. However, 'accessible' cobalt amount does not exceed 50% even in sample CA-II (Co:Al = 1). Reducibility of Co^{2+} species is dramatically improved, when Mg^{2+} or Zn^{2+} cation are introduced into the catalyst support. Actually, promoter cations replace inactive Co^{2+} cations. However, this advantage of promotion with Mg^{2+} and Zn^{2+} is accompanied by a significant increase in the size of metallic cobalt particles. Therefore, promoted catalysts selectivity is much worse than that of non-promoted ones.

Sample N/CA combines a low reducibility of CA samples with a low dispersion of metal Co particles in promoted catalysts. This may be reasonably explained by the presence of two almost independent phases, namely, Co_3O_4 and support CA, which comprise the N/CA sample.

Temperature dependence of CA samples activity (estimated by two points for sample CA and by five points for samples CA-I and CA-II) agrees well with the literature data on the apparent activation energy of CO conversion (14–16 kcal mol^{-1}) [30,32] and CH_4 formation (25–30 kcal mol^{-1}) [33]. The same seems to be valid for catalyst P/MA. However, sample N/CA exhibits a 'zero' apparent activation energy for both CO conversion and CH_4 formation. Moreover, activity of sample P/ZA at 503 K is significantly less than at 483 K. P/ZA testing was trice repeated (including the independent activation procedure), and showed same temperature dependence each time.

Table 5
Catalytic performance of the studied Co/Al catalysts, reduced at 600°C

Sample	CA	CA-I	CA-II	N/CA	P/MA	P/ZA
Co loading (wt.%)[a]	37	46	54	54	29	24
Amount of 'accessible' Co^0 (with respect to Co loading)[a]	15	30	51	30	78	77
Co^0 particle size (nm)[b]	5–6	4–5[c]	6–7[c]	15	11	9
Dispersion of Co^0[d]	0.20	0.23	0.17	0.07	0.11	0.13
Amount of surface Co^0 (μmol Co^0 s g^{-1} cat)	180	570	701	435	428	350
$T = 483$ K						
CO conversion rate (μmol g^{-1} cat h^{-1})	560	730	1340	730	830	920
CO conversion rate (mmol g^{-1} (accessible Co^0) h^{-1})	10.5	5.3	4.9	2.0	3.4	5.8
CO conversion TOF (10^{-4} mol per Co atm s^{-1})	8.6	3.6	4.7	4.7	5.6	7.3
CH_4 formation rate (μmol g^{-1} cat h^{-1})	160	90	180	270	290	250
CH_4 formation TOF (10^{-5} mol per Co atm s^{-1})	25	4.6	6.1	17	19	20
ASF parameter α for saturated C_3–C_8	0.84	0.89	0.84	0.79	0.81	0.81
ASF parameter α for olefins C_3–C_8	0.76	0.84	0.81	0.74	0.78	0.76
Ratio of propene to propane	1.2	4	2	0.9	1.1	1
$T = 503$ K						
CO conversion rate (μmol g^{-1} cat h^{-1})	1090	1490	1880	740	1170	650
CO conversion rate (mmol g^{-1} (accessible Co^0) h^{-1})	20.6	10.7	6.8	2.0	5.1	4.1
CO conversion TOF (10^{-4} mol per Co atm s^{-1})	17	7.3	6.6	4.7	7.6	5.2
CH_4 formation rate (μmol g^{-1} cat h^{-1})	340	260	610	360	640	330
CH_4 formation TOF (10^{-4} mol per Co atm s^{-1})	5.2	1.3	2.1	2.3	4.2	2.6
ASF parameter α for saturated C_3–C_8	0.72	0.72	0.69	0.66	0.68	0.68
ASF parameter α for olefins C_3–C_8	0.68	0.67	0.62	0.60	0.64	0.58
Ratio of propene to propane	1.3	1.4	2	1.3	1.2	0.4

[a] From the STA data (see the text).
[b] From the TEM data.
[c] From the XRD data on the $(1\,1\,1)_{fcc}$ peak broadening.
[d] The ratio of the surface metal atoms amount to the total amount of metal atoms was estimated from the experimental value of the average particle diameter, *d*, considering the cuboctahedral shape of a particle, as it was made in [29].

3.2.2. Catalytic tests of the catalysts reduced at 470–480°C

The results of catalytic testing of catalysts reduced at 470–480°C in pure hydrogen flow are present in Tables 6 and 7. The footnotes for these tables are the same as for Table 5.

1. Sample N/CA reduced at 480°C performs similarly to sample reduced at 600°C. The activity of sample reduced at 480°C related to 1 g of catalyst was found to be lower than that of sample reduced at high temperatures. However, TOF values for CO conversion and CH_4 formation are very close to TOF values of N/CA reduced at 600°C. Thus, the observed difference in activities may be ascribed to the different extent of Co reduction.
2. Sample P/ZA reduced at 480°C exhibits extremely low activity in CO conversion. Traces of methane and light hydrocarbons were detected at a reaction temperature of 503 K. Product composition is close to that obtained over samples CA and CA-II reduced at 470 (see below).
3. Unpromoted samples CA and CA-II reduced at 470°C show activity (TOF of CO conversion) 10 times lower than that obtained over samples reduced at 600°C. FTS product composition differs significantly from that obtained over catalysts reduced at 600°C. Methane, ethylene and propylene are the main products at 503 K. TOF of CH_4 formation at 503 K is 10 times lower than that obtained over the catalysts reduced at 600°C. Reaction selectivity towards methane at 503 K is ca. 11 wt.% for CA-II and ca. 16% for CA reduced at 470°C. Paraffins C^{2+} comprise 35–50% of the overall CO conversion. Thus, conversion towards olefins is about 30% (as referred to carbon). No CO_2 is detected (sensitivity towards CO_2 is about 0.05 vol.% at the

Table 6
Catalytic performance of the studied Co/Al catalysts reduced at 480°C

Sample	CA	CA-II	N/CA	P/ZA
Co loading (wt %)[a]	37	54	54	24
Amount of 'accessible' Co^0, Co loading (%)[a]	6	19	40	61
Co^0 particle size (nm)[b]	5–6	4–5[c]	15	9
Dispersion of Co^0[d]	0.20	0.17	0.08	0.13
Amount of surface Co^0 (μmol Co^0 s g^{-1}cat)	115	290	330	230
$T = 483$ K				
CO conversion rate (μmol g^{-1} cat h^{-1})	~16	79	450	No testing at 483 K
CO conversion rate (mmol g^{-1} (accessible Co^0) h^{-1})	0.5	0.8	1.9	
CO conversion TOF (10^{-4} mol per Co atm s^{-1})	0.4	0.76	3.8	
CH_4 formation rate (μmol g^{-1} cat h^{-1})	3.6	26	110	
CH_4 formation TOF (10^{-5} mol per Co atm s^{-1})	0.9	2.25	9.2	
ASF parameter α for saturated C_3–C_8	–	0.65	0.77	
ASF parameter α for olefins C_3–C_8	–	0.65	0.69	
Ratio of propene to propane	1	3	1.7	
$T = 503$ K				
CO conversion rate (μmol g^{-1} cat h^{-1})	22	83	430	~20
CO conversion rate (mmol g^{-1} (accessible Co^0) h^{-1})	0.6	0.8	1.8	0.2
CO conversion TOF (10^{-4} mol per Co atm s^{-1})	0.53	0.81	3.6	0.24
CH_4 formation rate (μmol g^{-1} cat h^{-1})	3.2	9	110	2.6
CH_4 formation TOF (10^{-5} mol per Co atm s^{-1})	0.8	0.9	9.0	0.3
ASF parameter α for saturated C_3–C_8	–	0.67	0.66	–
ASF parameter α for olefins C_3–C_8	0.35	0.59	0.62	0.58
Ratio of propene to propane	1	3	1.5	1

[a] From the STA data (see the text).
[b] From the TEM data.
[c] From the XRD data on the $(1\,1\,1)_{fcc}$ peak broadening.
[d] The ratio of the surface metal atoms amount to the total amount of metal atoms was estimated from the experimental value of the average particle diameter, *d*, considering the cuboctahedral shape of a particle, as it was made in [29].

outlet, i.e. 3% of the CO conversion in the case). Additional data on the selectivity of samples P/ZA, CA and CA-II reduced at 470°C are presented in Table 7.

At 483 K, CA and CA-II are even more selective in the synthesis of olefins. Their selectivity towards olefins is about 50% (as referred to carbon). However, their activity in methane synthesis is higher, than that

Table 7
More data on the FTS synthesis selectivity over the samples, reduced at 470°C

Sample	CA (%)	CA-II (%)	P/ZA (%)
$T = 483$ K			
CH_4 selectivity (C basis)	22	32	No testing at 483 K
C_2H_4 selectivity (C basis)	32	13	
C_3H_6 selectivity (C basis)	13	14	
C_{4+} olefins selectivity (C basis)	5	16	
$T = 503$ K			
CH_4 selectivity (C basis)	16	11	14
C_2H_4 selectivity (C basis)	24	7.5	8.9
C_3H_6 selectivity (C basis)	13	10	4.5
C_{4+} olefins selectivity (C basis)	12	23	17

at 503 K, while their activity towards paraffins C^{2+} is lower. Regarding the fraction of saturated hydrocarbons products one may notice a low value of parameter α. Amazingly, α-values for olefin fraction obtained over CA-II and P/ZA are high enough (0.65 at 483 K).

Note that it is often supposed, that C_2H_4 re-adsorbs and incorporates rapidly into the hydrocarbon intermediates on the surface of Co^0. Normally, apparent molecular rate for C_2H_4 to form is three to five times lower than that for C_3H_6. Over catalysts in concern, the ethylene formation molecular rate significantly exceeds the rate of propylene formation.

4. Discussion

According to the data described above properties of Co–Al precipitated catalysts change dramatically, if their reduction temperature is elevated to 600°C. The catalytic properties of precipitated samples reduced at temperature below 500°C differ a lot from the properties of samples reduced at 600°C. In addition, catalytic properties of promoted samples reduced at 600°C slightly differ from those of unpromoted samples also reduced at 600°C. The structures of their active components seem to be similar, and their dispersion is of the same order of magnitude. Therefore, it is reasonable to ascribe the observed difference in the catalytic properties to non-similarity in the structure of catalysts under discussion and first and foremost of their support structure and composition.

1. 'Spinel-like' phase of non-reduced samples contains a lot of Co^{2+}, OH^- and CO_3^{2-}. The amount of anionic admixtures may be roughly estimated from the STA data on the weight loss during reduction at 600°C (Table 3). The amount of Co^{2+} can be estimated from the data on the reduction capability of cobalt cations (Table 4). Estimation results are given in Table 8. Cations Co^{2+} occupy both octahedral and tetrahedral sites in the CA-* samples, and mostly the octahedral sites in promoted samples.
2. Reduction at low temperatures (below 500°C) causes no significant removal of anionic admixtures from the support. However, there is some discrepancy between the data on reduction degree, estimated from the weight loss during the low-temperature reduction and the data, estimated from the weight gain during the oxidation of samples CA and P/MA. This discrepancy might indicate a partial removal of anionic admixtures from the sample to occur. We may suppose that support structure does not change during the low-temperature reduction. We intend to ascribe it to the removal of similar admixtures from the structure of the CoO and $Co_xMg_{1-x}O$ phases during Co^{2+} reduction in these oxides. An anion-exchanged structure of these oxides was proved earlier in [34].
3. During reduction at 600°C, the octahedral Co^{2+} species of the support are reduced in CA-* samples; while groups OH^- and CO_3^{2-} leave the

Table 8
Comparison of the support ionic composition and the chemical properties of the studied catalysts

Sample	CA, CA-II[a] reduced at 480°C	CA-samples reduced at 600°C	P/ZA, P/MA, reduced at 600°C
Support composition			
Co^{2+}/Al^{3+} ratio	0.9–1.3	0.6–0.8	0
Co^{2+} location	Octahedrons and tetrahedrons	Mostly tetrahedrons	None
OH^- and CO_3^{2-} content	High	Medium	Low
Temperature of Co^0 oxidation (°C)	250–450	50–250	50–250
Catalytic properties (483 K)			
TOF of CO conversion	$2–7 \times 10^{-5}$	$4–6 \times 10^{-4}$	$5–8 \times 10^{-4}$
TOF of methane formation	$0.5–2 \times 10^{-5}$	$5–6 \times 10^{-5}$	$2–3 \times 10^{-4}$
Selectivity to C_2H_4 (C basis) (%)	13–30	1–3	<1
Selectivity to olefins (C basis) (%)	40–55	25–35	15–25
The value of α for paraffins	Low	High	High

[a] P/ZA was not tested in the FTS at 483 K, however it exhibited the similar performance at 503 K.

structure. However, in this case weight loss during reduction is much less than by the sample promoted by Mg^{2+} and Zn^{2+}. One may suppose that there is still a lot of anionic admixtures in the structure of Co–Al support. Actually, the IR spectra of samples registered after catalytic tests show, that in samples CA-* support still has structure $\{Me^{2+}{}_xAl^{2+}{}_xO_{3+y-z}(OH)_{2y}(CO_3{}^{2-})_z\}$. Band at ca. 800 cm^{-1} decreases and shifts to lower frequencies for samples P/ZA and P/MA. However, it remains distinct for samples CA. Note that if groups OH^- and $CO_3{}^{2-}$ are present in the sample after reduction, values of specific activities (TOF values) of catalysts are slightly underestimated.

4. Cations Co^{2+} are totally reduced at 600°C in promoted samples P/ZA and P/MA; content of groups OH^- and $CO_3{}^{2-}$ being rather low (IRS data).

The data in Table 8 reveal correlation between the amount of anionic admixtures in the support and the properties of Co–Al precipitated catalysts. The properties of samples seem to have no correlation with amount of Co^{2+} in the support. However, amount of Co^{2+} in octahedral coordination may correlate with the catalytic properties, since there are no Co^{2+} in the high-temperature reduced samples and, vice versa, there is a lot of Co^{2+} in the octahedral coordination in the support of samples reduced at low temperatures. Certain amount of octahedron coordinated Co^{2+} cations might be present in unpromoted (CA-*) samples reduced at 600°C. More definite conclusions need further detailed studies by means of DRS UV–VIS, XPS and other techniques [35,36].

Lapidus and coauthors reported in [1] on band 2050 cm^{-1} in the IR spectra of the CO molecules adsorbed on the surface of impregnated Co/Al_2O_3 samples. They assign these vibrations to CO molecules adsorbed on the surface of the Co^0 particles, possessing a 'less marked electron-donor capability' or '$Co^{\delta+}$', particles. In [37], Kadinov et al. attributed similar absorption band to the $Co^{\delta+}$–CO species of Co/Al_2O_3 catalysts reduced at 723 K.

The presence of such species in the Co/Al_2O_3 catalysts allows us to make a tentative supposition, that reported above catalytic properties of samples reduced at temperatures below 500°C are related to the a transfer of positive charge onto metallic Co particles. Apparently, this supposition needs verification by special tests [35].

5. Conclusions

1. The transformation of hydrotalcite-type structure into Me^{2+} aluminate during calcination proceeds gradually through an inverted spinel structure with a composition of $(Me^{2+}{}_{1-x}Al^{3+}{}_x)(Me^{2+}{}_xAl^{3+}{}_{2-x})O_{4-2y-z}(OH)_{2y}(CO_3{}^{2-})_z$. Spinel phase structure inversion is supposed to be thermodynamically favorable only due to the presence of some anionic admixtures.
2. Reduction of Co^{2+} species, located in the octahedron sites of inverted spinel phase (support), occurs at 580–620°C, and is accompanied by anionic admixtures removal from the spinel structure.
3. Promotion of Co–Al catalysts with Mg^{2+} or Zn^{2+} increases the extent of Co^{2+} reduction up to 100%.
4. A highly dispersed Co^0 phase is present in all reduced co-precipitated catalysts tested. Poor support crystallinity most likely helps to avoid the formation of well-crystallized metallic cobalt particles.
5. Catalytic properties of Co–Al catalysts promoted with Mg (or Zn) and reduced at 600°C are similar to those, expected for the dispersed Co^0 particles according to the literature data.
6. The catalytic properties of unpromoted Co catalysts reduced at 600°C differ from those of catalysts promoted by Mg (Zn) by a slightly lower specific activity, a higher selectivity towards olefins and a lower selectivity towards methane. Active component dispersion in unpromoted catalysts is higher, Co reduction degree is lower. The resulting performance of these catalysts is far worse than that of promoted catalysts.
7. Reduction temperature strongly affects the catalytic properties of Co–Al catalysts. The catalytic properties of the Co–Al catalysts reduced at 470–480°C are dramatically different from those of same catalysts reduced at 600°C. A miserable activity, and an abnormally high selectivity towards olefins, including (surprisingly) ethylene, are characteristic for these samples.
8. The obtained data allow us to suppose that the observed difference in the catalytic properties

can be related to the different structure of studied catalysts and first and foremost to their support structure and composition. The difference of catalytic properties may be caused by a transfer of positive charge onto metal Co particles in the Co–Al samples reduced at low temperatures. However, further investigations are needed to elucidate the nature of the active component–support interaction.

Acknowledgements

This research work was implemented by the finance by PEC, Japan.

References

[1] R. Oukaci, A.H. Singleton, J.A. Goodwin Jr., Appl. Catal. A: Gen. 186 (1999) 129.
[2] A. Lapidus, A. Krylova, V. Kazanskii, V. Borovikov, A. Zaitsev, J. Rathousky, A. Zukai, M. Jancalkowa, Appl. Catal. 73 (1991) 65.
[3] S. Vada, A. Hoff, E. Adnanes, D. Schanke, A. Holmen, Top. Catal. 2 (1995) 155.
[4] A.M. Hilmen, D. Schanke, A. Holmen, Catal. Lett. 38 (1996) 143.
[5] J. van de Loosdrecht, Preparation and properties of supported Fischer–Tropsch catalysts, Ph.D. thesis, Universiteit Utrecht, Utrecht, The Netherlands, 1995 (Chapter 3).
[6] J. van de Loosdrecht, M. van der Haar, A.M. van der Kraan, A.J. van Dillen, J.W. Geus, Appl. Catal. A: Gen. 150 (1997) 365.
[7] Y.L. Zhang, D.G. Wei, S. Hammache, J.G. Goodwin, J. Catal. 188 (1999) 281.
[8] P. Arnoldy, J.A. Moulijn, J. Catal. 93 (1985) 38.
[9] D.A.M. Monti, A. Baiker, J. Catal. 83 (1983) 323.
[10] B. Ernst, S. Libs, P. Chaumette, A. Kiennemann, Appl. Catal. A: Gen. 186 (1999) 145.
[11] T.A. Krieger, L.M. Plyasova, T.M. Yurieva, Mater. Sci. Forum 321–324 (1) (1999) 386.
[12] P.A. Ramachandran, R.V. Chaudhari, Three-Phase Catalytic Reactors, Gordon and Breach, New York, 1983.
[13] J.T. Kloprogge, R.L. Frost, Appl. Catal. A: Gen. 184 (1999) 61.
[14] M.J. Hernandez-Moreno, M.A. Ulibarri, J.L. Rendon, C.J. Serna, Phys. Chem. Miner. 12 (1985) 34.
[15] S. Kannan, C.S. Swamy, J. Mater. Sci. Lett. 11 (1992) 1585.
[16] K. Nakamoto, Infrared and Raman Spectra of Inorganic and Coordination Compounds, Wiley, New York, 1986.
[17] PCPDF Win, Ver 1.30, JCPDS ICDD, Swarthmore, PA, USA, 1997, pp. 36–1451.
[18] PCPDF Win, Ver 1.30, JCPDS ICDD, Swarthmore, PA, USA, 1997, pp. 4–829.
[19] PCPDF Win, Ver 1.30, JCPDS ICDD, Swarthmore, PA, USA, 1997, pp. 9–402.
[20] O.V. Makarova, G.V. Kharlamov, L.M. Plyasova, Izv. SO AN SSSR, Chem. Ser. 3 (1990) 67.
[21] B.G. Erenburg, V.P. Fadeeva, A.I. Min'kov, L.M. Shadrina, Ye.A. Stoyanov, Izv. SO AN SSSR, Chem. Ser. 4 (2) (1981) 54.
[22] T.M. Yurieva, L.I. Kuznetsova, G.K. Boreskov, Kinet. Katal. 23 (2) (1982) 264.
[23] J. Preudhomme, P. Tarte, Spectrochem. Acta 27A (9) (1971) 1834.
[24] S. Hafner, F. Laves, Zeitschrift fur Kristallographie 115 (1961) 321.
[25] L.M. Plyasova, T.M. Yurieva, I.Yu. Molina, T.A. Kriger, A.M. Balagurov, L.P. Davydova, V.I. Zaikovskii, G.N. Kustova, V.V. Malakhov, L.S. Dovlitova, Kinet. Katal. 41 (2000) 472.
[26] R.J. Hill, J.R. Graig, G.V. Gibbs, Phys. Chem. Miner. 4 (1979) 317.
[27] O.V. Makarova, T.M. Yurieva, L.M. Plyasova, A.V. Ziborov, G.N. Kustova, G.V. Odegova, Kinet. Katal. 36 (5) (1995) 774.
[28] A. Navrotsky, O.J. Kleppa, J. Inorg. Nucl. Chem. 29 (1967) 2701.
[29] A. Barbier, E.B. Pereira, G.A. Martin, Catal. Lett. 45 (1997) 221.
[30] A.A. Khassin, T.M. Yurieva, V.N. Parmon, Doklady Phys. Chem. 367 (1–3) (1999) 213 (the official English translation from Doklady RAN 367 (3) (1999) 367).
[31] A.A. Khassin, V.N. Parmon, Doklady Phys. Chem. 368 (4–6) (1999) 283 (the official English translation from Doklady RAN 368 (4) (1999) 503).
[32] R.C. Baetzold, J. Phys. Chem. 88 (1984) 5583.
[33] M.A. Vannice, J. Catal. 37 (1975) 449.
[34] T.M. Yurieva, React. Kinet. Catal. Lett. 23 (1983) 267.
[35] A.A. Khassin, V.F. Anufrienko, T.V. Larina, T.M. Yurieva, V.N. Parmon, manuscript in preparation.
[36] A.A. Khassin, T.M. Yurieva, V.V. Kaichev, V.I. Bukhtiyarov, A.A. Budneva, Ye.A. Paukshtis, V.N. Parmon, manuscript in preparation.
[37] G. Kadinov, Ch. Bonev, S. Todorova, A. Palazov, J. Chem. Soc., Faraday Trans. 94 (1998) 3027.